ARTICLE

Phase Behavior and Ionic Conductivity of Concentrated Solutions of Polystyrene-Poly(ethylene oxide) Diblock Copolymers in an Ionic Liquid

Peter M. Simone[†] and Timothy P. Lodge[*,†,‡]

Department of Chemistry and Department of Chemical Engineering & Materials Science, University of Minnesota, Minneapolis, Minnesota 55455

ABSTRACT Concentrated solutions of poly(styrene-*b*-ethylene oxide) (PS-PEO) diblock copolymers were prepared using the ionic liquid 1-ethyl-3-methylimidazolium bis(trifluoromethylsulfonyl)imide [EMI][TFSI] as the solvent. The self-assembled microstructures adopted by the copolymer solutions have been characterized using small-angle X-ray scattering. Lyotropic mesophase transitions were observed, with a progression from hexagonally packed cylinders of PEO, to lamellae, to hexagonally packed cylinders of PS upon increasing [EMI][TFSI] content. The change in lamellar domain spacing with ionic liquid concentration was found to be comparable to that reported for other block copolymers in strongly selective solvents. The ionic conductivity of the concentrated PS-PEO/[EMI][TFSI] solutions was measured via impedance spectroscopy, and ranged from 1×10^{-7} to 1×10^{-3} S/cm at temperatures from 25 − 100 °C. Additionally, the ionic conductivity of the solutions was found to increase with both ionic liquid concentration and molecular weight of the PEO blocks. The ionic conductivity of PEO homopolymer/[EMI][TFSI] solutions was also measured in order to compare the conductivity of the PS-PEO solutions to the expected limit for a lamellar sample with randomly oriented microstructure grains.

KEYWORDS: ionic liquid • block copolymer • ionic conductivity • membrane • phase diagram

INTRODUCTION

Concentrated solutions of block copolymers adopt self-assembled microstructures akin to those of the bulk state (1). For A−B diblocks, the common microstructures observed include spherical domains situated in a cubic lattice (either bcc or fcc), hexagonally packed cylindrical domains, the bicontinuous gyroid, and lamellae. If the solvent used to prepare the solution is selective, the majority will partition into one of the block microdomains. This is analogous to a change in the block volume fraction of the copolymer (f), which drives the domain interfacial curvature toward the less soluble block domains. Additionally, the unfavorable interactions between the insoluble block and the selective solvent increases the effective degree of segregation (χN) between the domains, where χ is the Flory−Huggins interaction parameter between the (solvated) copolymer blocks and N is the degree of polymerization. These changes in the effective copolymer volume fraction and degree of segregation drive lyotropic mesophase transitions as the solution concentration is varied. The lamellar, gyroid, and cylindrical phases are all of potential interest as membrane materials.

The behavior of block copolymers upon addition of common organic and aqueous solvents has been extensively studied (2−11). Ionic liquids are a fairly new class of solvents that is attracting a high level of current research interest (12, 13). Ionic liquids are composed of ionic species that are generally large and asymmetric and possess delocalized charge. These characteristics result in a hindrance to the formation of well-ordered ionic lattices and result in low melting points for ionic liquids relative to more common ionic compounds. In addition to low melting points, ionic liquids also possess many other appealing properties, including negligible volatility, high thermal and electrochemical stability, and good ionic conductivity, which make them excellent candidates as electrolyte materials (14−16). Indeed, ionic liquids have been explored as electrolytes in various devices such as lithium ion batteries (17−23), fuel cells (24−31), and dye-sensitized solar cells (32). However, in many cases, a solid electrolyte material would be more robust and versatile, and thus there is interest in imparting solid structure to ionic liquids, while still maintaining their good conductivity. One route to a solid structure has been to blend ionic liquids with polymers to form so-called "ion gel electrolytes". Polymeric materials employed include homopolymers (33−36), typically poly(ethylene oxide), and copolymers (37−42), typically poly(vinylidene fluoride-*co*-hexafluoropropylene). Additionally, chemically (43−48) and physically (49−51) cross-linked polymer networks have been swollen with ionic liquids to form ion gels. Moreover, there have been multiple strategies reported for "gelling"

* Corresponding author.
Received for review August 20, 2009 and accepted December 2, 2009
† Department of Chemistry, University of Minnesota.
‡ Department of Chemical Engineering & Materials Science, University of Minnesota.
DOI: 10.1021/am900555f

Published on Web 12/10/2009

Table 1. Molecular Characteristics of PS-PEO Block Copolymers

copolymer	M_{PS} (kg/mol)[a]	M_{PEO} (kg/mol)	PDI[b]	f_{PEO}[c]
SO(20−5)	19.7	4.8	1.04	0.18
SO(20−6)	19.7	6.3	1.03	0.23
SO(20−8)	19.7	8.3	1.08	0.28
SO(20−13)	19.7	13.4	1.06	0.39

[a] M_{PS} determined by SEC with multiangle light scattering detection. [b] PDI determined by SEC calibrated with polystyrene standards. [c] f_{PEO} determined by ^{1}H NMR spectroscopy.

ionic liquids (52−55). It may also be beneficial if the material used to provide solid structure to the ionic liquid on the macroscale also possesses an ordered structure on the nanoscale. This has recently been demonstrated by the groups of Ohno and Kato, who utilized liquid crystalline materials that display hexagonal columnar and bicontinuous cubic structures (56−58). Similarly, block copolymers could also be used to impart nanoscale structure if the ionic liquid selectively partitions into one domain. We have previously studied the solvent selectivity and phase behavior of several poly(butadiene-*b*-ethylene oxide) (PB-PEO) diblock copolymers with the addition of ionic liquids, and found that the ionic liquids selectively solvate the PEO blocks of the copolymers, resulting in interesting lyotropic phase behavior (59). Here we describe the phase behavior of poly(styrene-*b*-ethylene oxide) diblock copolymers (PS-PEO) with the addition of the ionic liquid 1-ethyl-3-methylimidazolium bis(trifluoromethylsulfonyl)imide [EMI][TFSI]. This ionic liquid was chosen because it has been widely used in electrochemical applications and studies, mainly because of the stability and low viscosities (i.e., high ionic diffusion coefficients) of ionic liquids based on the [TFSI] anion. Additionally, we have used [EMI][TFSI] in previous studies and are thus familiar with its synthesis, characteristics, and successful methods for sample preparation. This ionic liquid behaves as a selective solvent for the PEO blocks of the copolymers and thus leads to lyotropic transitions. In addition, the ionic conductivity of the PS-PEO/[EMI][TFSI] solutions is also reported. The overall goal of this study is to understand the self-assembly behavior and ionic conductivity of block copolymer/ionic liquid solutions, with a view toward their potential use as microstructured electrolyte materials.

EXPERIMENTAL SECTION

Materials. The PS-PEO copolymers were synthesized via living anionic polymerization and the molecular characteristics are summarized in Table 1. The blocks were grown sequentially following an established procedure for polymerizing ethylene oxide blocks from polyalkane blocks (60). This method allowed synthesis of copolymers from the same parent PS block, and thus the PEO block length could be systematically varied while keeping the PS block constant. The absolute molecular weight of the parent PS block was determined via size exclusion chromatography (SEC) utilizing a multiple angle light scattering detector (DAWN DSP, Wyatt Technology Corp.). This M_{PS} was used along with ^{1}H NMR spectroscopy to determine the volume fraction of PEO (f_{PEO}) and thus the M_{PEO} for the diblocks. The overall polydispersity index (PDI) for the diblocks was determined via SEC calibrated with PS standards. One PEO homopolymer was ordered from Sigma, and used without further purification. The molecular weight of the PEO homopolymer was determined via SEC calibrated with PS standards. Universal calibration using the Mark−Houwink parameters for PS and PEO in chloroform gave a molecular weight of 9.1 kg/mol for the homopolymer. The [EMI][TFSI] was synthesized via anion exchange between 1-ethyl-3-methylimidazolium bromide [EMI][Br] (Solvent Innovation) and lithium bis(trifluoromethylsulfonyl)imide ([Li][TFSI]) (IoLiTec) in water at 70 °C for 12 h. After the ion exchange, the aqueous layer was removed and the ionic liquid was washed repeatedly with water. The ionic liquid was further purified by stirring over activated carbon. The final [EMI][TFSI] product was a clear, very faint yellow liquid. After purification, the ionic liquid was dried under a vacuum (ca. 50 mTorr) at 70 °C for 3 days and stored in a vacuum desiccator or in a glovebox under argon. Preparation of PS-PEO/[EMI][TFSI] solutions was performed as follows. The desired amounts of block copolymer and ionic liquid were measured gravimetrically into a vial and then codissolved in dichloromethane (ca. 5−10 wt % copolymer). The majority of the cosolvent was removed slowly (36−48 h) with stirring under dry nitrogen purge. Subsequently, the copolymer solutions were dried under vacuum (ca. 50 mTorr) at 60 °C until constant weight was reached (ca. 48 h). Finally, the solutions were annealed at 150 °C for 1 h. After preparation, the solutions were stored in a vacuum desiccator.

Small-Angle X-ray Scattering. Small-angle X-ray scattering (SAXS) experiments were performed at the DuPont−Northwestern−Dow collaborative access team (DND-CAT) beamline at the Advanced Photon Source, Argonne National Laboratories. The PS-PEO/[EMI][TFSI] samples were loaded into hermetically sealed, differential scanning calorimetry (DSC) pans, which were heated and cooled in a Linkam DSC sample holder during scattering experiments. Before collecting scattering patterns, all samples were heated to 200 °C for 5−10 min and then patterns were collected upon cooling the sample. Two-dimensional scattering patterns were recorded by a Mar CCD area detector, and then azimuthally integrated to give one-dimensional scattering data as intensity (I) vs wave-vector ($q = 4\pi \sin(\theta/2)/\lambda$), where θ is the scattering angle (calibrated with silver behenate) and λ is the X-ray wavelength. The X-ray wavelengths used were 0.8856 and 0.7293 Å, and the sample to detector distances were 6.5 and 8.5 m.

AC Impedance Spectroscopy. The ionic conductivity was measured via AC impedance spectroscopy, using a Solartron 1255B frequency response analyzer connected to a Solartron SI 1287 electrochemical interface. The solutions were hot-pressed at 150 °C into a Teflon ring, which held the samples at a constant diameter (7 mm) and thickness (2 mm). The sample disks were sandwiched between two stainless steel blocking electrodes. The AC amplitude was 10 mV and the frequency was scanned from 1×10^6 to 1 Hz. The conductivity of the solutions was calculated from the complex impedance ($Z^* = Z' - iZ''$). The high-frequency plateau in the real impedance (Z') was taken as the bulk resistance (R) of the sample, and the conductivity was calculated as

$$\sigma = \frac{L}{RA} \tag{1}$$

where L is the sample thickness and A is the electrode contact area. The conductivity cell constant (L/A) was calibrated using a 3.5 mM aqueous KCl solution standard (Fluka Analytical) with an ionic conductivity of 5 μS/cm at 25 °C. The estimated error in all the ionic conductivity values presented is ±10%, based on experimental reproducibility.

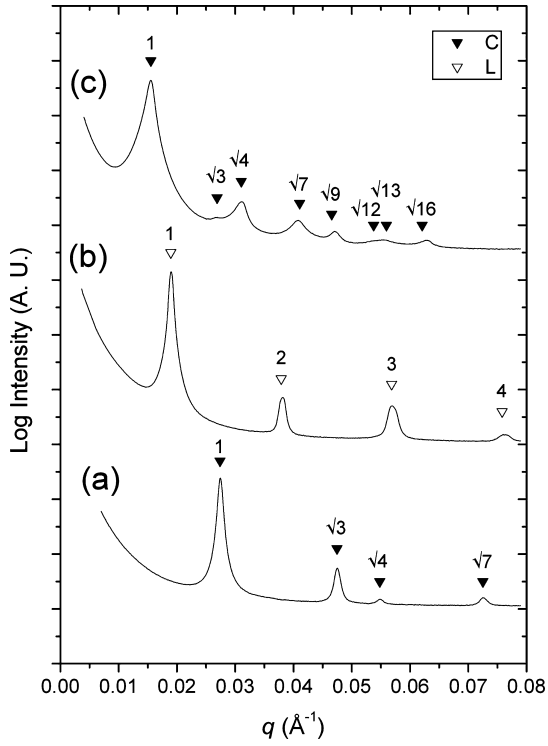

FIGURE 1. Representative 1D SAXS plots for PS-PEO/[EMI][TFSI] solutions at 150 °C: (a) SO(20−5) $\phi = 0.93$; (b) SO(20−8) $\phi = 0.76$; (c) SO(20−8) $\phi = 0.49$. Filled triangles correspond to expected intensity maxima for C at q/q^* values of 1:√3:√4:√7:√9:√12:√13:√16, and open triangles correspond to expected intensity maxima for L at q/q^* values of 1:2:3:4.

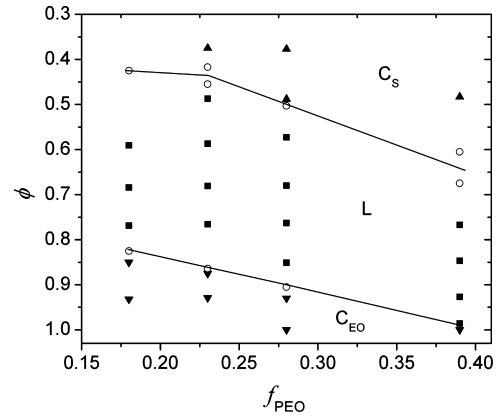

FIGURE 2. Phase map for PS-PEO/[EMI][TFSI] solutions at 150 °C. The *x*-axis corresponds to volume fraction of EO in the bulk copolymers. The *y*-axis is solution concentration given as copolymer volume fraction. Regions of hexagonally packed EO cylinders (C_{EO}, ▼), lamellae (L, •), and hexagonally packed styrene cylinders (C_S, ▲) are denoted. Open circles (○) represent solutions that assemble into coexisting L and C microstructures. Solid lines represent estimated phase boundaries included to guide the eye.

RESULTS AND DISCUSSION

Phase Behavior. Figure 1 shows 1D SAXS patterns collected at 150 °C, which are representative of those used to map the microstructure phase behavior of the PS-PEO/[EMI][TFSI] solutions. The scattered intensity maxima are referenced by the q/q^* ratios corresponding to the allowed Bragg reflections for the ordered copolymer microstructures, where q^* is the position of the primary scattering peak. Figure 2 shows the phase map for the PS-PEO/[EMI][TFSI] solutions at 150 °C. The *x*-axis of the phase map corresponds to the volume fraction of PEO in the neat copolymers; thus, each vertical series of points represents the phase behavior of one of the PS-PEO copolymers with increasing [EMI][TFSI] content. The scattering patterns for the neat SO(20−5) diblock did not display any long-range order at any of the temperatures investigated (200−30 °C). Similarly, the scattering patterns for the SO(20−6) diblock at elevated temperatures (≥100 °C) did not display long-range order. The order−disorder transition temperatures of the copolymers were not explicitly characterized; however, at room temperature SO(20−6) displays a weak scattering pattern corresponding to a hexagonally packed cylinder microstructure (C_{EO}). The subscript designates which copolymer block forms the minority (cylinder) domain. The low degree of segregation observed for the SO(20−5) and SO(20−6) copolymers is not surprising, because of the low value of χ between PS and PEO (~0.08 at 25 °C) (61). Upon addition of ionic liquid, both SO(20−5) and SO(20−6) solutions with ϕ of 0.93 adopt a C_{EO} microstructure, and do not display any thermotropic order−order or order−disorder transitions between 30 and 200 °C. Likewise, no thermotropic order−order or order−disorder transitions were observed in the 30−200 °C temperature range for any of the PS-PEO/[EMI][TFSI] solutions investigated. This indicates a large increase in the degree of segregation between microstructure domains upon addition of the [EMI][TFSI] solvent, which is selective for the PEO blocks. Here it is important to note that SAXS does not provide direct evidence of the partitioning of the ionic liquid into the PEO domains of the copolymer microstructure. However, based on the fact that PEO homopolymers are readily soluble in [EMI][TFSI] and PS homopolymers are not, and on the solubility behavior of similar block copolymers in ionic liquids (49, 59), we can take [EMI][TFSI] to be a selective solvent for the PEO blocks of the copolymers. Thus, as the concentration of ionic liquid is increased, the PEO blocks are swollen and the interfacial curvature is driven toward the PS domains. Thus, a lyotropic C_{EO} to L transition is observed. Eventually, upon addition of sufficient [EMI][TFSI], an L to C_S transition occurs, which represents a "phase inversion" to a hexagonal cylinder microstructure in which the longer PS blocks form the minority domain.

If we use the qualitative assumption that increasing the ionic liquid concentration is analogous to a simple increase in f_{PEO}, then a prediction of the phase behavior for the solutions can be estimated by following a simple horizontal path across the theoretical χN vs f phase diagram for A−B diblocks (62). This method is often referred to as the trajectory approach (5, 63). Starting in the region of C_{EO} on the theoretical phase diagram and moving horizontally to the C_S region, the anticipated microstructure progression would be $C_{EO} \rightarrow G_{EO} \rightarrow L \rightarrow G_S \rightarrow C_S$. The gyroid microstructure is not definitively observed for any of the PS-PEO solutions investigated. Evidence for the possible coexistence of the gyroid along with lamellae and hexagonally packed cylinders is seen in the scattering pattern obtained for the SO(20−13)/[EMI][TFSI] solution with ϕ of 0.68 (Figure 3a). The shoulder

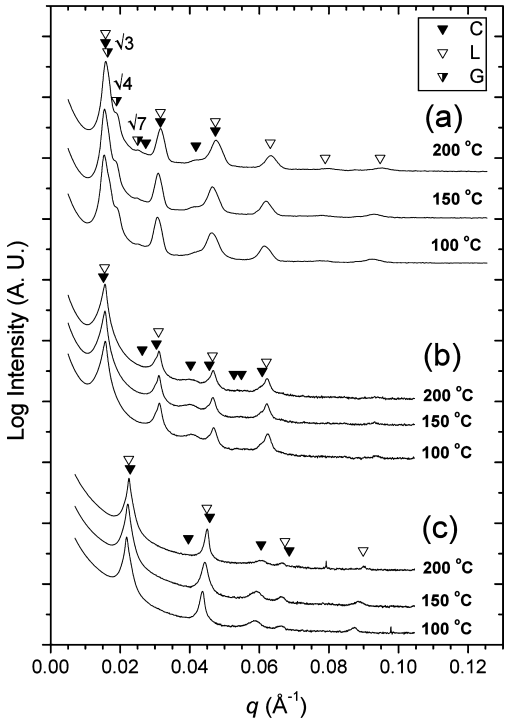

FIGURE 3. Representative 1D SAXS plots for PS-PEO/[EMI][TFSI] solutions displaying coexisting microstructures: (a) SO(20−13) $\phi = 0.68$; b) SO(20−8) $\phi = 0.50$; (c) SO(20−8) $\phi = 0.91$. Filled triangles correspond to expected intensity maxima for C at q/q^* values of $1:\sqrt{3}:\sqrt{4}:\sqrt{7}:\sqrt{9}:\sqrt{12}:\sqrt{13}:\sqrt{16}$, open triangles correspond to expected intensity maxima for L at q/q^* values of 1:2:3:4:5:6, and half filled triangles correspond to expected intensity maxima for G, where the primary peak position is taken as $\sqrt{3}$ and the secondary peak positions are referenced to q/q^* ratios of $\sqrt{4}$ and $\sqrt{7}$.

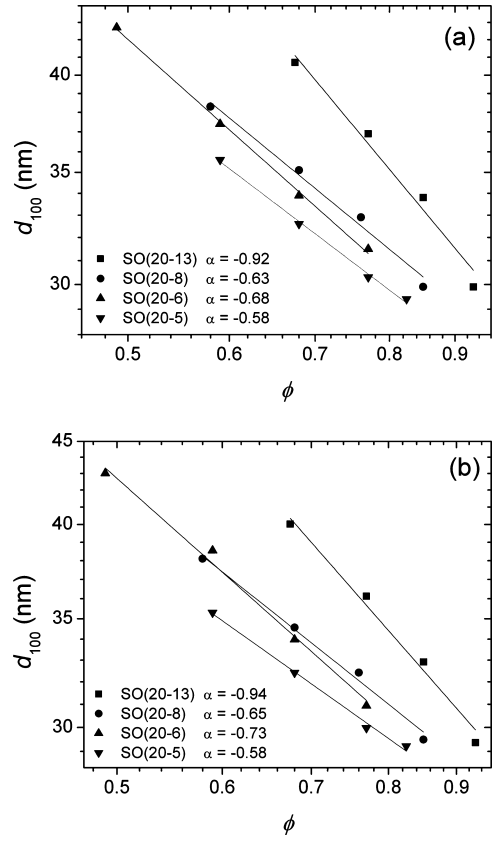

FIGURE 4. Log−log plots of lamellar domain spacing (d_{100}) versus solution concentration, given as copolymer volume fraction (ϕ). Solid lines represent power law fits ($d \sim \phi^{\alpha}$). (a) 150 and (b) 200 °C.

on the primary scattering peak in the 0.68 pattern can be referenced to the $\sqrt{4}$ scattering peak consistent with the gyroid, and a weak peak corresponding to the $\sqrt{7}$ reflection is also observed. The scattering peaks corresponding to the coexisting L, C, and G persisted at all temperatures investigated. The solutions were annealed at 150 °C for 1 hour prior to preparation of the SAXS samples, and for approximately 10 min at each temperature before collecting SAXS patterns. Thus, the coexisting L, C, and G microstructures appear to be at least metastable. However, longer-term annealing experiments are necessary before solid conclusions can be made about the thermodynamic stability of these microstructures. Overall, coexisting C and L microstructures were observed for solutions in the region of the phase map where gyroid would be expected (i.e., between regions of C and L). The scattering patterns for the SO(20−8) 0.50 and 0.91 volume fraction solutions shown in Figures 3b and c are representative of those observed for solutions which possess coexisting C and L microstructure (open symbols in Figure 2). Similar results have been reported for other diblock copolymer solutions with strongly selective solvents, and have been attributed to destabilization of the gyroid microstructure due to an increase in chain packing frustration with increasing degree of segregation (6, 63, 64). The solvent provides an extra degree of freedom, allowing the formation of coexisting C/L instead of G.

A measure of the degree of segregation for the PS-PEO/[EMI][TFSI] solutions can be obtained from the change in domain spacing (d) with solution concentration. Dilution of a segregated copolymer with a neutral good solvent (i.e., equal solvation of both blocks) screens the unfavorable interactions between the blocks and results in a decrease in domain spacing due to relaxation of chain stretching normal to the domain interface. Conversely, addition of a selective solvent to a block copolymer results in a drive to decrease the interfacial area, in order to reduce the number of unfavorable contacts between the insoluble block and the solvent. This brings about increased chain stretching normal to the interface, and thus an increase in the domain spacing. Figure 4 shows double logarithmic plots of the lamellar domain spacing (d_{100}) versus solution concentration, given as copolymer volume fraction (ϕ), for the PS-PEO/[EMI][TFSI] solutions. The lamellar domain spacing was calculated as $d_{100} = 2\pi/q^*$, where q^* is the position of the primary 100 lamellar scattering peak in the 1D SAXS patterns. The addition of the selective [EMI][TFSI] solvent results in an increase in domain spacing and thus negative values for α. For the PS-PEO/[EMI][TFSI] solutions the most negative α value was found to be −0.94 for SO(20−13) at 200 °C. This is consistent with the experimental results of Hanley et al. (63, 65) and Lai et al. (66), who studied the change in domain spacing for various poly(styrene-*b*-isoprene) diblocks (PS-PI) in selective solvents. Lai reported $\alpha = -1.03$ for PS-PI in the strongly isoprene selective solvent squalane, and Hanley found $\alpha = -0.61$ for PS-PI in the strongly styrene selective solvent dimethyl phthalate (DMP). Additionally, through self-

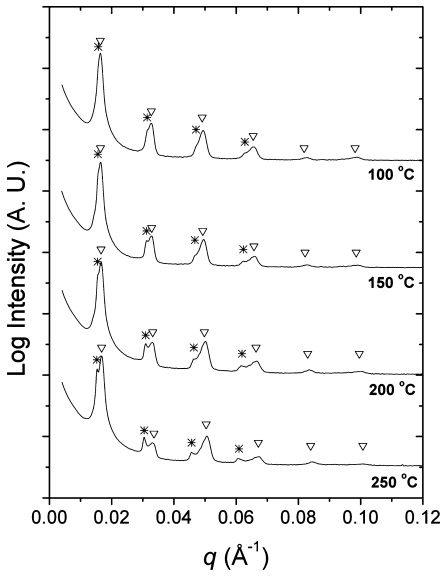

FIGURE 5. 1D SAXS patterns for SO(20−8) solution with $\phi = 0.57$. Patterns collected on cooling from 250 °C. Annealing time at each temperature was approximately 10 min. Arrowheads and asterisks mark expected reflections for lamellar microstructure ($q/q^* = 1{:}2{:}3{:}4$ ...).

consistent mean-field analysis of a lamellar forming diblock, Hanley et al. showed that $\alpha = -0.20$ for a strongly selective solvent (χ between solvent and insoluble block equal to 1). Thus, our experimental results imply that [EMI][TFSI] is behaving with a higher degree of selectivity than the theoretical case calculated by Hanley et al. (i.e., χ between the solvent and the insoluble block greater than 1), and that the large majority of the ionic liquid partitions into the PEO domains. Moreover, in a recent report closely related to the present study, Virgili et al. investigated the microstructure domain spacing vs solution concentration for a poly(styrene-*b*-2-vinylpyridine) diblock (PS-P2 VP) diluted with the ionic liquid imidazolium bis(trifluoromethylsulfonyl)imide ([Im][TFSI]) (67). The researchers report large, negative values of −2.31 and −3.16 at 145 and 225 °C, respectively. These results are qualitatively similar to ours, in that addition of the ionic liquid solvent results in negative values of α. However, the values reported by Virgili are much more negative than those obtained in the present study, which is potentially a result of the limited concentration range ($0.93 \leq \phi \leq 1.0$) over which the lamellar domain spacing could be measured in the PS-P2 VP/[Im][TFSI] solutions.

Another notable feature of the phase behavior of several of the PS-PEO/[EMI][TFSI] solutions was the presence of coexisting lamellar microstructures possessing different domain spacing. As shown in Figure 5, two distinct sets of scattering peaks are observed for the SO(20−8) solution with ϕ of 0.57. Similar patterns with coexisting lamellar scattering peaks were observed for the SO(20−6) 0.59 and 0.68 volume fraction solutions as well. The heating and annealing procedure employed while collecting the SAXS patterns in Figure 5 was as follows. The solutions were initially heated to 250 °C and annealed for 10 min prior to collecting the scattering pattern. The samples were then cooled and annealed for an additional 10 min at each subsequent temperature before collecting the scattering patterns. Thus, the total annealing time at elevated temperature (≥100 °C) was approximately 40−50 min (accounting for 1−2 min cooling time between temperatures). For the SO(20−8) solution with ϕ of 0.57, the lamellar microstructure with larger domain spacing (lower q) begins to yield to the phase possessing lower domain spacing as the sample is annealed. The SO(20−6) 0.59 and 0.68 volume fraction solutions show a smaller change in the relative intensities of the peaks corresponding to the two different lamellar microstructures.

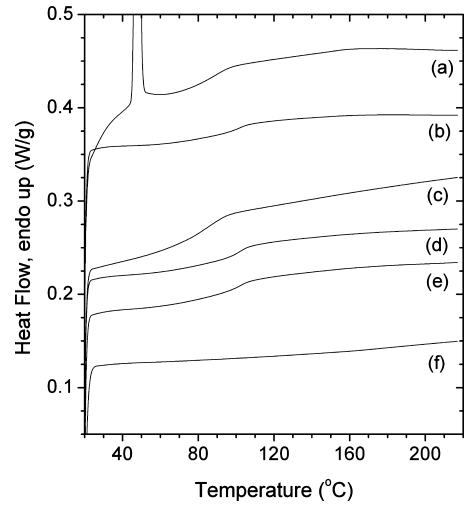

FIGURE 6. DSC thermograms: (a) SO(20−8) $\phi = 1.0$; b) SO(20−8) $\phi = 0.57$, $r = 0.40$; c) SO(20−6) $\phi = 1.0$; d) SO(20−6) $\phi = 0.68$, $r = 0.31$; e) SO(20−6) $\phi = 0.59$, $r = 0.46$; f) PEO $\phi = 0.38$, $r = 0.25$. Ion content (r) is the ratio of [EMI] cations to EO monomers in solution. All traces are second heating scans at a rate of 10 °C/min.

Coexisting lamellar microstructures have also been reported by Virgili et al. for a (PS-P2 VP) diblock copolymer diluted with the ionic liquid ([Im][TFSI]) (67), and by Young et al. for PS-PEO copolymers doped with lithium salts (68, 69). Virgili et al. proposed that the coexisting lamellar microstructures are a result of two coexisting phases possessing unequal amounts of ionic liquid. On the basis of DSC experiments showing well-defined crystalline melting peaks, Young was able to characterize the coexisting microstructures as arising from the crystallization of PEO−salt complexes. For the latter system, the crystallized PEO−salt complexes corresponded to the lamellar microstructure with larger domain spacing.

DSC experiments were conducted with the three PS-PEO/[EMI][TFSI] solutions that displayed coexisting lamellar microstructures. The DSC traces are plotted in Figure 6 for the SO(20−8) 0.57 volume fraction solution, and the SO(20−6) 0.59 and 0.68 volume fraction solutions. DSC traces for the neat SO(20−8) and SO(20−6) copolymers and for a 0.38 volume fraction solution of 9.1 kg/mol PEO homopolymer in [EMI][TFSI] are included in Figure 6 for comparison. For the 0.38 volume fraction PEO solution the ion content (r), taken as the ratio of [EMI] cations to PEO ether oxygen atoms (i.e., EO monomer units) in solution, is 0.25. Ion content is calculated from the measured polymer concentration using the bulk densities of PS (1.05 g/cm^3), PEO (1.13 g/cm^3), and [EMI][TFSI] (1.52 g/cm^3), and the copolymer

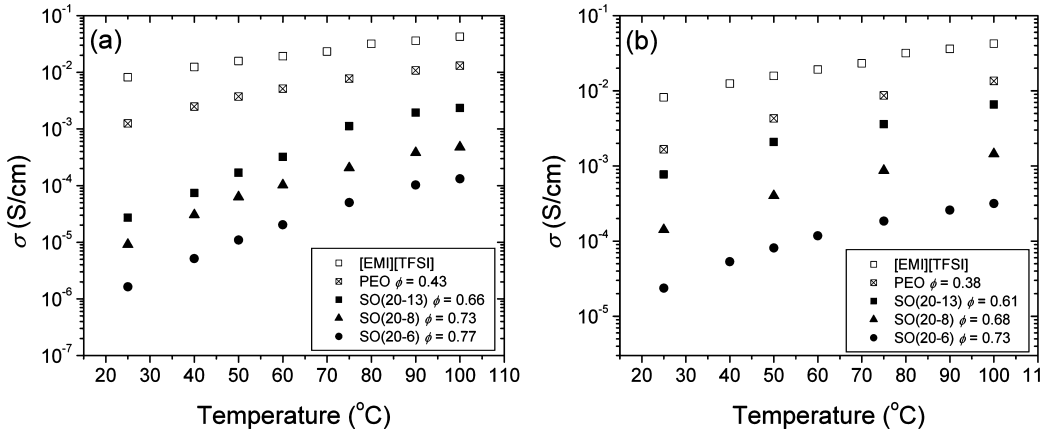

FIGURE 7. Conductivity vs temperature for PS-PEO/[EMI][TFSI] and PEO/[EMI][TFSI] solutions. (a) $r = 0.20$; (b) $r = 0.25$.

molecular volume fractions given in Table 1. For the SO(20−8) 0.57 and SO(20−6) 0.59 and 0.68 volume fraction solutions, r is equal to 0.40, 0.46, and 0.31, respectively. Thus the PEO homopolymer solution serves as a close comparison to the solvated state of the PEO blocks of the PS-PEO/[EMI][TFSI] solutions. All of the DSC traces in Figure 6 represent second heating scans, where the heating and cooling rates for all scans were 10 °C/min. The DSC samples were heated from 25 to 215 °C, then cooled back to 25 °C, and finally reheated to 215 °C. The hold times at the minimum and maximum temperatures were one minute for all the heating scans. The DSC results in Figure 6 show no evidence of a crystalline melting peak for the PS-PEO/[EMI][TFSI] solutions or for the PEO homopolymer solution. Only a slight increase in T_g is observed for the copolymer solutions, as compared to the neat copolymers. This is consistent with the results of Virgili et al., who also observed a slight increase in T_g for PS-P2 VP/[Im][TFSI] solutions as compared to the bulk PS-P2 VP. Thus, we do not observe any evidence that the formation of crystalline PEO-ionic liquid complexes is responsible for the coexisting lamellar microstructures observed via SAXS. However, the formation of crystalline PEO−ionic liquid complexes cannot be completely ruled out based on these results. The large size and asymmetry of many ionic liquid constituent ions result in inefficient crystal packing. Thus, slow crystallization of PEO−ionic liquid complexes may preclude the observance of crystallization and melting via DSC.

It should be noted that the lamellar domain spacing for the three PS-PEO/[EMI][TFSI] solutions displaying coexisting lamellar microstructures were included in the double logarithmic plots of d_{100} vs ϕ in Figure 4. For the SO(20−6) solutions with ϕ of 0.59 and 0.68, the difference in the domain spacing for the coexisting lamellar microstructures is small (≤1.0 nm). Thus, using either the higher or lower domain spacing value did not change the α value obtained from the power law fits for the SO(20−6) solutions. However, the difference in domain spacing for the coexisting lamellar microstructures in the SO(20−8) 0.57 volume fraction solution is ∼3 nm at 200 °C and ∼2 nm at 150 °C, which resulted in different values of α depending on which domain spacing is used in the fits. In the SAXS patterns collected for the SO(20−8) 0.57 volume fraction solution, the scattering peaks corresponding to the lamellar microstructure with lower domain spacing become dominant with annealing. Thus, the lower lamellar domain spacing was used in the plots of d_{100} vs ϕ for the SO(20−8) and SO(20−6) solutions shown in Figure 4.

Ionic Conductivity. The ionic conductivity of [EMI][TFSI], PEO solutions, and PS-PEO solutions was measured via AC impedance spectroscopy. Figures 7a and b show representative σ vs T data for neat [EMI][TFSI], and concentrated solutions of PEO homopolymer and PS-PEO copolymers with ion content equal to 0.20 and 0.25, respectively. At these concentrations, the SO(20−6) and SO(20−8) solutions fall in the L microstructure region of the PS-PEO/[EMI][TFSI] phase map, and the SO(20−13) solutions fall in a region of the phase map characterized by coexisting L and C_S microstructure. In general, for all the PS-PEO solutions investigated, σ ranged from 1×10^{-7} to 1×10^{-3} S/cm at temperatures from 25−100 °C. Here we note that conductivity values are not reported for SO(20−5)/[EMI][TFSI] because of general difficulty in preparing samples for impedance measurements using the hot-pressing method described in the experimental section. Samples prepared using solutions of the three other PS-PEO copolymers uniformly filled the Teflon spacer ring with no visible cracks or bubbles. For the SO(20−5) solutions, many samples were prepared and almost all possessed visible cracks and other inhomogeneities after hot-pressing, which is presumably due to the higher content of the brittle PS block in the SO(20−5) copolymer.

The ionic conductivity of the PS-PEO solutions is less than that of the PEO solutions and the neat ionic liquid at all temperatures. This is expected due to the randomly oriented lamellar domains that limit the direct ionic conduction through the sample. Simple geometric arguments predict for materials with randomly oriented lamellar domains that the ultimate conductivity for the sample is 2/3 of the maximum conductivity for the conducting phase (70), which is calculated as

$$\sigma_{max} = \phi_{CP}\sigma_{CP} \quad (2)$$

where ϕ_{CP} is the volume fraction of the conducting phase (PEO plus ionic liquid) and σ_{CP} is the conductivity of the conducting phase, taken as the measured conductivity of the

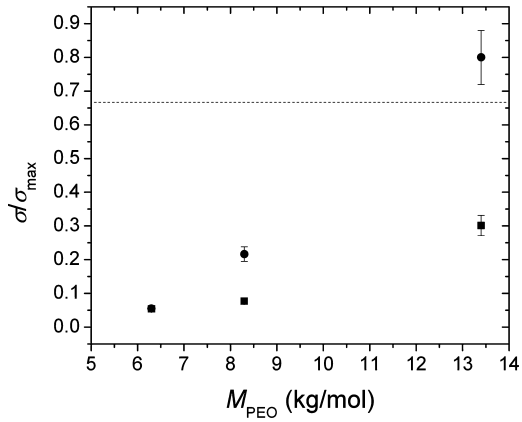

FIGURE 8. Normalized ionic conductivity (σ/σ_{max}) at 100 °C vs molecular weight of the copolymer PEO block. σ is the measured conductivity of the PS-PEO/[EMI][TFSI] solutions with $r = 0.20$ (■) and $r = 0.25$ (●). σ_{max} is calculated from eq 2.

PEO homopolymer/[EMI][TFSI] solution. Figure 8 shows the normalized ionic conductivity (σ/σ_{max}) at 100 °C vs molecular weight of the PEO blocks (M_{PEO}) for PS-PEO/[EMI][TFSI] solutions with ion content equal to 0.20 and 0.25. As the molecular weight of the PEO blocks increases, it can be seen that the normalized conductivity approaches the predicted limit of 2/3. Note that the SO(20−13)/[EMI][TFSI] solutions with ion content equal to 0.20 ($\phi = 0.66$) and 0.25 ($\phi = 0.61$) fall in the region of the PS-PEO/[EMI][TFSI] solution microstructure phase map (Figure 2) characterized by coexisting L and C_S. In the C_S microstructure, the PS blocks from the cylindrical domains, while the majority, matrix domain is formed by the PEO blocks plus the ionic liquid. Thus, the C_S microstructure should display higher ionic conductivity, which is not limited to the predicted 2/3 maximum for the lamellar microstructure. It is likely that the presence of a coexisting hexagonal cylinder phase results in the normalized conductivity above the 2/3 limit for the SO(20−13)/[EMI][TFSI] solution with r equal to 0.25. Additionally, a portion of the increase in normalized conductivity for the SO(20−13)/[EMI][TFSI] solution with r equal to 0.20 may also be attributed to the presence of a hexagonal cylinder phase coexisting with lamellae. However, a recent study by Wanakule et al. reports that the normalized ionic conductivity for several PS-PEO diblock copolymers doped with [Li][TFSI] is independent of transitions in the copolymer microstructure (71). Thus, further investigations of the affects of copolymer microstructure on the ionic conductivity in PS-PEO/[EMI][TFSI] solutions may be warranted.

The PS-PEO/[EMI][TFSI] ionic conductivity results can be compared with those of Singh et al. and Panday et al. who have recently reported on the ionic conductivity of PS-PEO diblocks doped with [Li][TFSI] (72, 73). The closest comparison to our SO(20−13) copolymers is an SO(16−16) diblock with r equal to 0.02 and 0.085, where the reported σ/σ_{max} ratio is approximately 0.1−0.15 for both ion content values. However, these researchers showed normalized conductivity values approaching the 2/3 limit as M_{PEO} increased, with the limit ultimately being reached for copolymers with $M_{PEO} > 60$ kg/mol. Thus, we expect similar behavior in our PS-PEO/[EMI][TFSI] solutions, where increasing M_{PEO} of the diblocks could lead to higher ionic conductivity and σ/σ_{max} values approaching 2/3 for samples possessing lamellar microstructure.

Figures 9a and b show ionic conductivity of the PS-PEO solutions vs M_{PEO} at $r = 0.20$ and 0.25, respectively. As can be seen, the ionic conductivity of the copolymer solutions increases with M_{PEO}. The studies of Singh and Panday discussed previously also report increasing ionic conductivity with M_{PEO} for PS-PEO diblocks doped with [Li][TFSI]. These authors have attributed the increase in conductivity to an increase in ionic dissociation at the center of the conductive PEO domains. This is reasoned to be a result of a gradient in the dielectric constant of the PEO domains, with the value increasing toward the center of the domains. The increase in dielectric constant stems from an increase in chain conformational freedom with increasing distance from the domain interface, where the PEO chains have a more highly stretched conformation. Indeed, Gomez et al. have observed localization of ions at the center of the PEO domains using energy-filtered transmission electron microscopy (74). It is conceivable that similar effects result in the increase in conductivity with M_{PEO} observed in our PS-PEO/[EMI][TFSI] solutions.

Figures 10a−d shows σ vs r for PEO homopolymer, SO(20−13), SO(20−8), and SO(20−6) solutions, respectively. The ionic conductivity for the PEO homopolymer and the PS-PEO copolymer solutions increases with ion content for all the concentrations measured. Similar results were observed by Chen et al. for poly(methyl methacrylate) homopolymer (PMMA) and a random PMMA-*r*-PS copolymer diluted with [EMI][TFSI] (42). In comparison, PEO doped with atomic ions (e.g., Li^+ salts) shows a maximum in ionic conductivity with increasing r. This result has been observed in both PEO homopolymers (75) and copolymers containing PEO blocks (72). Initially, at low values of r, increasing ion content leads to higher conductivity due to an increase in the number of charge carriers. However, at higher values of r a decrease in conductivity is observed because of ion pairing and transient cross-linking of the PEO chains due to strong coordination with the cations. Conversely, the large size, asymmetry, and charge delocalization of the ionic liquid ions potentially leads to weaker ion-dipole interactions with the PEO chains. In other words, the same characteristics that lead to low ionic liquid melting points, allows for increasing ionic conductivity with r. This is supported by recently reported molecular dynamics simulations of electrolytes based on PEO and ionic liquids (76), where the researchers found decreased interaction strength between PEO and the large ions of an ionic liquid, as compared to Li^+. This study involved the ionic liquids 1,3-dimethylimidazolium hexafluorophosphate [MMI][PF_6] and 1-butyl-3-methylimidazolium hexafluorophosphate [BMI][PF_6]. Although these ionic liquids differ from that used in the present study, we believe parallels can safely be drawn because the nature of the interactions depends mostly on the cations and the PEO chains. Thus, we anticipate [EMI] to behave similarly to [MMI] and [BMI].

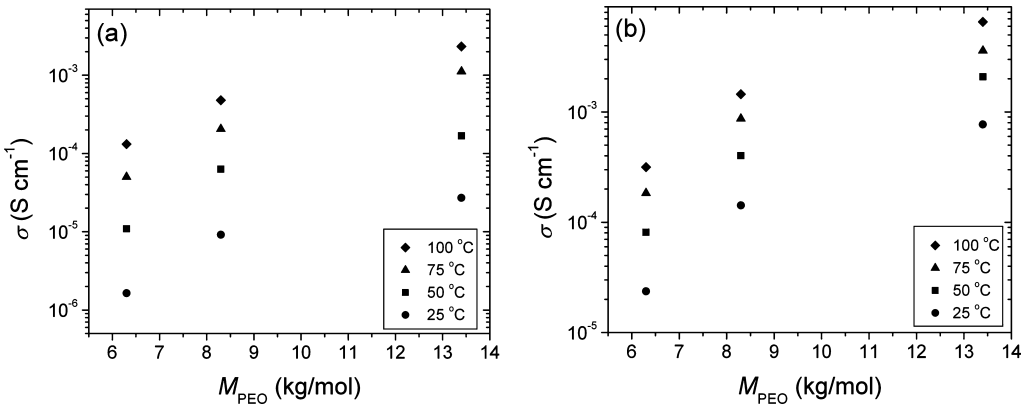

FIGURE 9. Ionic conductivity vs PEO block molecular weight (M_{PEO}). (a) $r = 0.20$; (b) $r = 0.25$.

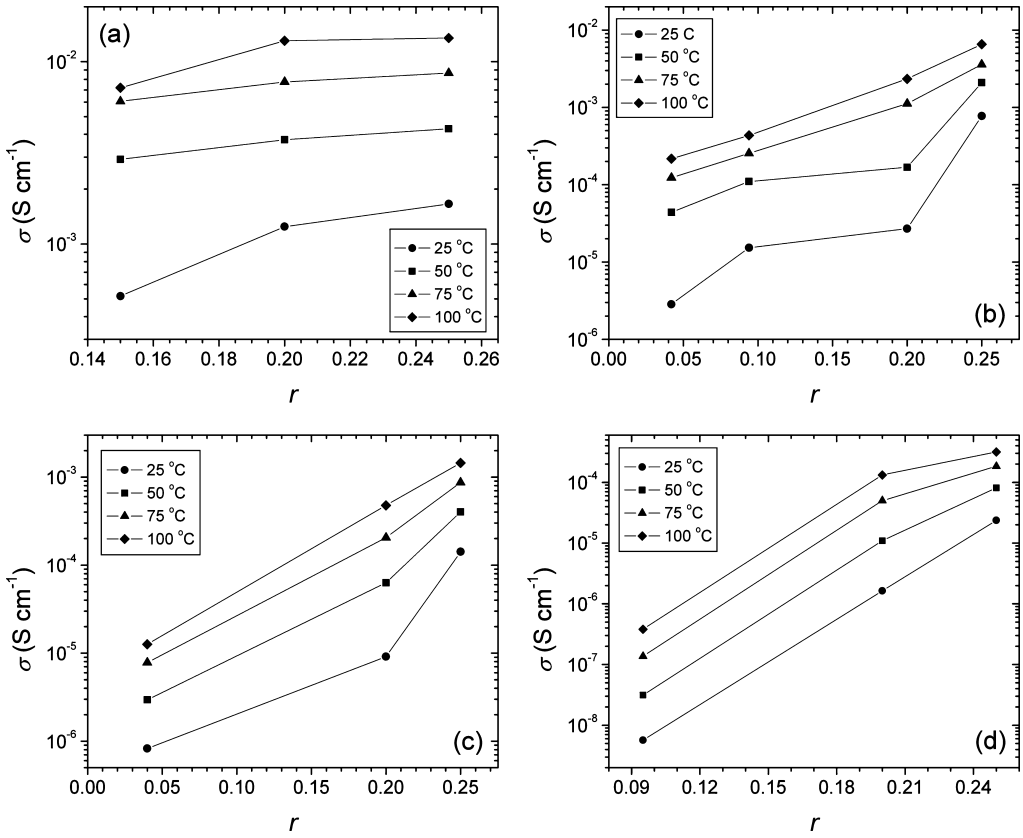

FIGURE 10. Ionic conductivity vs r. (a) PEO homopolymer; (b) SO(20−13); (c) SO(20−8); (d) SO(20−6).

CONCLUSION

Concentrated solutions of PS-PEO in [EMI][TFSI] possess well-defined nanostructure that can be tuned by simply adjusting solution concentration. [EMI][TFSI] is found to be strongly selective for PEO, and thus the ionic liquid is confined to the microstructure adopted by the PEO domains of the copolymer. These simple nanostructured electrolyte materials displayed ionic conductivities in the range of 1×10^{-3} S/cm at 100 °C, and show further promise due to their increasing ionic conductivity with both ion concentration and M_{PEO}. One drawback for these materials is a limit in their ultimate conductivity due to the randomly oriented microstructure grains inherent in the bulk samples. Thus efforts are ongoing to align the electrolyte microstructure in order to improve the ultimate ionic conductivity attainable for these materials.

Acknowledgment. This work was supported by the National Science Foundation, through Awards DMR-0406656 and DMR-0804197. Use of the Advanced Photon Source was supported by the U.S. Department of Energy, Office of Science, Office of Basic Energy Sciences, under Contract DE-AC02-06CH11357. We thank Phil Bühlmann for use of the impedance analyzer.

REFERENCES AND NOTES

(1) Hamley, I. W. *The Physics of Block Copolymers*; Oxford University Press: Oxford, U.K., 1998.
(2) Lodge, T. P.; Hanley, K. J.; Pudil, B.; Alahapperuma, V. *Macromolecules* **2003**, *36*, 816–822.
(3) Lodge, T. P.; Pudil, B.; Hanley, K. J. *Macromolecules* **2002**, *35*, 4707–4717.
(4) Lai, C.; Russel, W. B.; Register, R. A. *Macromolecules* **2002**, *35*, 841–849.
(5) Sadron, C.; Gallot, B. *Makromol. Chem.* **1973**, *164*, 301–332.

(6) Hajduk, D. A.; Kossuth, M. B.; Hillmyer, M. A.; Bates, F. S. *J. Phys. Chem. B* **1998**, *102*, 4269–4276.
(7) Shibayama, M.; Hashimoto, T.; Kawai, H. *Macromolecules* **1983**, *16*, 16–28.
(8) Jain, S.; Dyrdahl, M. H. E.; Gong, X.; Scriven, L. E.; Bates, F. S. *Macromolecules* **2008**, *41*, 3305–3316.
(9) Wanka, G.; Hoffmann, H.; Ulbricht, W. *Macromolecules* **1994**, *27*, 4145–4159.
(10) Messé, L.; Corvazier, L.; Young, R. N.; Ryan, A. J. *Langmuir* **2002**, *18*, 2564–2570.
(11) Hamley, I. W.; Mai, S.-M.; Ryan, A. J.; Fairclough, J. P.; Booth, C. *Phys. Chem. Chem. Phys.* **2001**, *3*, 2972–2980.
(12) Wasserscheid, P.; Welton, T., Eds. *Ionic Liquids in Synthesis*, 2nd ed.; Wiley-VCH: Weinheim, Germany, 2008.
(13) Weingärtner, H. *Angew. Chem., Int. Ed.* **2007**, *46*, 2–19.
(14) Ohno, H., Ed. *Electrochemical Aspects of Ionic Liquids*; John Wiley & Sons: Hoboken, NJ, 2005.
(15) Galiński, M.; Lewandowski, A.; Stepniak, I. *Electrochim. Acta* **2006**, *51*, 5567–5580.
(16) Fernicola, A.; Scrosati, B.; Ohno, H. *Ionics* **2006**, *12*, 95–102.
(17) Seki, S.; Ohno, Y.; Miyashiro, H.; Kobayashi, Y.; Usami, A.; Mita, Y.; Terada, N.; Hayamizu, K.; Tsuzuki, S.; Watanabe, M. *J. Electrochem. Soc.* **2008**, *155*, A421–A427.
(18) Seki, S.; Ohno, Y.; Kobayashi, Y.; Miyashiro, H.; Usami, A.; Mita, Y.; Tokuda, H.; Watanabe, M.; Hayamizu, K.; Tsuzuki, S.; Hattori, M.; Terada, N. *J. Electrochem. Soc.* **2007**, *154*, A173–A177.
(19) Hayashi, K.; Nemoto, Y.; Akuto, K.; Sakurai, Y. *J. Power Sources* **2005**, *146*, 689–692.
(20) Garcia, B.; Lavallée, S.; Perron, G.; Michot, C.; Armand, M. *Electrochim. Acta* **2004**, *49*, 4583–4588.
(21) Sakaebe, H.; Matsumoto, H.; Tatsumi, K. *J. Power Sources* **2005**, *146*, 693–697.
(22) Ishikawa, M.; Sugimoto, T.; Kikuta, M.; Ishiko, E.; Kono, M. *J. Power Sources* **2006**, *162*, 658–662.
(23) Matsumoto, H.; Sakaebe, H.; Tatsumi, K.; Kikuta, M.; Ishiko, E.; Kono, M. *J. Power Sources* **2006**, *160*, 1308–1313.
(24) Angell, C. A.; Byrne, N.; Belieres, J.-P. *Acc. Chem. Res.* **2007**, *40*, 1228–1236.
(25) Xu, W.; Angell, C. A. *Science* **2003**, *302*, 422–425.
(26) Nakamoto, H.; Watanabe, M. *Chem. Commun.* **2007**, 2539–2541.
(27) Nakamoto, H.; Noda, A.; Hayamizu, K.; Hayashi, S.; Hamaguchi, H.; Watanabe, M. *J. Phys. Chem. C* **2007**, *111*, 1541–1548.
(28) Matsuoka, H.; Nakamoto, H.; Susan, M. A. B. H.; Watanabe, M. *Electrochim. Acta* **2005**, *50*, 4015–4021.
(29) Noda, A.; Susan, M. A. B. H.; Kudo, K.; Mitsushima, S.; Hayamizu, K.; Watanabe, M. *J. Phys. Chem. B* **2003**, *107*, 4024–4033.
(30) Susan, M. A. B. H.; Noda, A.; Mitsushima, S.; Watanabe, M. *Chem. Commun.* **2003**, 938–939.
(31) Ogihara, W.; Kosukegawa, H.; Ohno, H. *Chem. Commun.* **2006**, 3637–3639.
(32) Gorlov, M.; Kloo, L. *Dalton Trans.* **2008**, 2655–2666.
(33) Lewandowski, A.; Świderska, A. *Solid State Ionics* **2004**, *169*, 21–24.
(34) Shin, J.-H.; Henderson, W. A.; Tizzani, C.; Passerini, S.; Jeong, S.-S.; Kim, K.-W. *J. Electrochem. Soc.* **2006**, *153*, A1649–A1654.
(35) Zhu, C.; Cheng, H.; Yang, Y. *J. Electrochem. Soc.* **2008**, *155*, A569–A575.
(36) Kim, Y. H.; Cheruvally, G.; Choi, J. W.; Ahn, J. H.; Kim, K. W.; Ahn, H. J.; Choi, D. S.; Song, C. E. *Macromol. Symp.* **2007**, *249–250*, 183–189.
(37) Sutto, T. E. *J. Electrochem. Soc.* **2007**, *154*, P101–P107.
(38) Fuller, J.; Breda, A. C.; Carlin, R. T. *J. Electrochem. Soc.* **1997**, *144*, L67–L70.
(39) Yeon, S.-H.; Kim, K.-S.; Choi, S.; Cha, J.-H.; Lee, H. *J. Phys. Chem. B* **2005**, *109*, 17928–17935.
(40) Singh, B.; Sekhon, S. S. *Chem. Phys. Lett.* **2005**, *414*, 34–39.
(41) Bansal, D.; Cassel, F.; Croce, F.; Hendrickson, M.; Plichta, E.; Salomon, M. *J. Phys. Chem. B* **2005**, *109*, 4492–4496.
(42) Chen, H.; Gwee, L.; Choi, J.-H.; Salas de la Cruz, D.; Winey, K. I.; Elabd, Y. A. *PMSE Prepr.* **2009**, *100*, 696–697.
(43) Klingshirn, M. A.; Spear, S. K.; Subramanian, R.; Holbrey, J. D.; Huddleston, J. G.; Rogers, R. D. *Chem. Mater.* **2004**, *16*, 3091–3097.
(44) Noda, A.; Watanabe, M. *Electrochim. Acta* **2000**, *45*, 1265–1270.
(45) Susan, M. A. B. H.; Kaneko, T.; Noda, A.; Watanabe, M. *J. Am. Chem. Soc.* **2005**, *127*, 4976–4983.
(46) Rupp, B.; Schmuck, M.; Balducci, A.; Winter, M.; Kern, W. *Eur. Polym. J.* **2008**, *44*, 2986–2990.
(47) Tigelaar, D. M.; Meador, M. A. B.; Bennett, W. R. *Macromolecules* **2007**, *40*, 4159–4164.
(48) Tiyapiboonchaiya, C.; MacFarlane, D. R.; Sun, J.; Forsyth, M. *Macromol. Chem. Phys.* **2002**, *203*, 1906–1911.
(49) He, Y.; Boswell, P. G.; Bühlmann, P.; Lodge, T. P. *J. Phys. Chem. B* **2007**, *111*, 4645–4652.
(50) He, Y.; Lodge, T. P. *Chem. Commun.* **2007**, 2732–2734.
(51) He, Y.; Lodge, T. P. *Macromolecules* **2008**, *41*, 167–174.
(52) Shimano, S.; Zhou, H.; Honma, I. *Chem. Mater.* **2007**, *19*, 5216–5221.
(53) Ueno, K.; Hata, K.; Katakabe, T.; Kondoh, M.; Watanabe, M. *J. Phys. Chem. B* **2008**, *112*, 9013–9019.
(54) Hanabusa, K.; Fukui, H.; Suzuki, M.; Shirai, H. *Langmuir* **2005**, *21*, 10383–10390.
(55) Kawauchi, T.; Kumaki, J.; Okoshi, K.; Yashima, E. *Macromolecules* **2005**, *38*, 9155–9160.
(56) Yoshio, M.; Kagata, T.; Hoshino, K.; Mukai, T.; Ohno, H.; Kata, T. *J. Am. Chem. Soc.* **2006**, *128*, 5570–5577.
(57) Ichikawa, T.; Yoshio, M.; Hamasaki, A.; Mukai, T.; Ohno, H.; Kato, T. *J. Am. Chem. Soc.* **2007**, *129*, 10662–10663.
(58) Shimura, H.; Yoshio, M.; Hoshino, K.; Mukai, T.; Ohno, H.; Kato, T. *J. Am. Chem. Soc.* **2008**, *130*, 1759–1765.
(59) Simone, P. M.; Lodge, T. P. *Macromolecules* **2008**, *41*, 1753–1759.
(60) Hillmyer, M. A.; Bates, F. S. *Macromolecules* **1996**, *29*, 6994–7002.
(61) Cochran, E. W.; Morse, D. C.; Bates, F. S. *Macromolecules* **2003**, *36*, 782–792.
(62) Cochran, E. W.; Garcia-Cervera, C. J.; Fredrickson, G. H. *Macromolecules* **2006**, *39*, 2449–2451.
(63) Hanley, K. J.; Lodge, T. P.; Huang, C.-I. *Macromolecules* **2000**, *33*, 5918–5931.
(64) Matsen, M. W.; Bates, F. S. *Macromolecules* **1996**, *29*, 7641–7644.
(65) Hanley, K. J. Block Copolymers: Phase Behavior in Neutral and Selective Solvents. Ph.D. Thesis, University of Minnesota, Twin Cities, MN, 2001.
(66) Lai, C.; Russel, W. B.; Register, R. A. *Macromolecules* **2002**, *35*, 4044–4049.
(67) Virgili, J. M.; Hexemer, A.; Pople, J. A.; Balsara, N. P.; Segalman, R. A. *Macromolecules* **2009**, *42*, 4604–4613.
(68) Young, W.-S.; Brigandi, P. J.; Epps, T. H. *Macromolecules* **2008**, *41*, 6276–6279.
(69) Young, W.-S.; Epps, T. H. *Macromolecules* **2009**, *42*, 2672–2678.
(70) Sax, J.; Ottino, J. M. *Polym. Eng. Sci.* **1983**, *23*, 165–176.
(71) Wanakule, N. S.; Panday, A.; Mullin, S. A.; Gann, E.; Hexemer, A.; Balsara, N. P. *Macromolecules* **2009**, *42*, 5642–5651.
(72) Singh, M.; Odusanya, O.; Wilmes, G. M.; Eitouni, H. B.; Gomez, E. D.; Patel, A. J.; Chen, V. L.; Park, M. J.; Fragouli, P.; Iatrou, H.; Hadjichristidis, N.; Cookson, D.; Balsara, N. P. *Macromolecules* **2007**, *40*, 4578–4585.
(73) Panday, A.; Mullin, S.; Gomez, E. D.; Wanakule, N.; Chen, V. L.; Hexemer, A.; Pople, J.; Balsara, N. P. *Macromolecules* **2009**, *42*, 4632–4637.
(74) Gomez, E. D.; Panday, A.; Feng, E. H.; Chen, V.; Stone, G. M.; Minor, A. M.; Kisielowski, C.; Downing, K. H.; Borodin, O.; Smith, G. D.; Balsara, N. P. *Nano Lett.* **2009**, *9*, 1212–1216.
(75) Robitaille, C. D.; Fauteux, D. *J. Electrochem. Soc.* **1986**, *133*, 315–325.
(76) Costa, L. T.; Ribeiro, M. C. C. *J. Chem.Phys.* **2007**, *127*, 164901.

AM900555F